THE NIGHT-SKY AT THE CALAR ALTO OBSERVATORY

S.F SÁNCHEZ[1], J. ACEITUNO[1], U. THIELE[1], D. PÉREZ-RAMÍREZ[2,3], J. ALVES[1]
Draft version February 1, 2008

ABSTRACT

We present a characterization of the main properties of the night-sky at the Calar Alto observatory for the time period between 2004 and 2007. We use optical spectrophotometric data, photometric calibrated images taken in moonless observing periods, together with the observing conditions regularly monitored at the observatory, such as atmospheric extinction and seeing. We derive, for the first time, the typical moonless night-sky optical spectrum for the observatory. The spectrum shows a strong contamination by different pollution lines, in particular from Mercury lines, which contribution to the sky-brightness in the different bands is of the order of $\sim$0.09 mag, $\sim$0.16 mag and $\sim$0.10 mag in B, V and R respectively. Regarding the strength of the Sodium pollution line in comparison with the airglow emission, the observatory does not fulfill the IAU recomendations of a dark site. The zenith-corrected values of the moonless night-sky surface brightness are 22.39, 22.86, 22.01, 21.36 and 19.25 mag arcsec^{-2} in U, B, V, R and I, which indicates that Calar Alto is a particularly dark site for optical observations up to the I-band. The fraction of astronomical useful nights at the observatory is $\sim$70%, with a $\sim$30% of photometric nights. The typical extinction at the observatory is $\kappa_V \sim$0.15 mag in the Winter season, with little dispersion. In summer the extinction has a wider range of values, although it does not reach the extreme peaks observed at other sites. The analysis of the Winter and summer extinction curves indicates that the Rayleigh scattering is almost constant along the year. The rise of the extinction in the summer season is due to an enhance of the Aerosol extinction, most probably associated with an increase of dust in the atmosphere. The median seeing for the last two years (2005-6) was $\sim$0.90″, being smaller in the Summer ($\sim$0.87″) than in the Winter ($\sim$0.96″).
We conclude in general that after 26 years of operations Calar Alto is still a good astronomical site. Its main properties are similar in many aspects to those of other major observatories where 10m-like telescopes are under operation or construction, being a natural candidate for future large aperture optical telescopes.

Subject headings: Astronomical Phenomena and Seeing

1. INTRODUCTION

The night sky brightness, the number of clear nights, the seeing, transparency and photometric stability are some of the most important parameters that qualify a site for front-line ground-based astronomy. There is limited control over all these parameters, and only in the case of the sky brightness is it possible to keep it at its natural level by preventing light pollution from the immediate vicinity of the observatory. Previous to the installation of any observatory, extensive tests of these parameters are carried out in order to find the best locations, maximizing then the efficiency of these expensive infraestructures. However, most of these parameters are not constant along the time. An example of this can be seen in the seeing evolution of the Paranal observatory, which is worse now than when the decision to built it at its current location was taken[4]. This is not an untypical situation.

We have started a program to determine the actual values of the main observing conditions for the Calar

Alto observatory. The Calar Alto observatory is located at 2168m height above the sealevel, in the Sierra de los Filabres (Almeria-Spain) at $\sim$45 km from the Mediterranean sea. It is the second largest european astronomical site in the north hemisphere, just behind the Observatorio del Roque de los Muchachos (La Palma), and the most important in the continental europe. Currently there are six telescopes located in the complex, three of them operated by the Centro Astronomico Hispano Aleman A.I.E. (CSIC-MPG), including the 3.5m, the largest telescope in the continental europe.

Along its 26 years of operations there has been different attempts to characterize some of the main properties described before: (i) Leinert et al. (1995) determined the sky brightness corresponding to the year 1990; (ii) Hopp & Fernandez (2002) studied the extinction curve corresponding to the years 1986-2000; (iii) Ziad et al. (2005) estimated the median seeing in the observatory from a single campain in may 2002. However, there is a need for a consistent study of all these properties, spanning over a similar time period.

In this article we study the main characteristics of the night-sky at the observatory including: (i) the night-sky spectrum, identifing the natural and light pollution emission lines and their strength, (ii) the moonless night-sky brightness in different bands, (iv) the extinction and its yearly evolution and (v) the atmospheric seeing and its yearly evolution. The study is limited to the last four years, with mostly corresponds to a period of minimun

[1] Centro Astronómico Hispano Alemán, Calar Alto, (CSIC-MPG), C/Jesús Durbán Remón 2-2, E-04004 Almeria, Spain
[2] Departamento de Física Aplicada, Facultad de Ciencias, Universidad de Granada,8 Fuentenueva s/n, 18071, Granada (Spain)
[3] Centro Andaluz de Medio Ambiente, Universidad de Granada. Junta de Andalucía, Avda. del Mediterraneo s/n. 18006 Granada (Spain).
Electronic address: sanchez@caha.es

[4] http://www.eso.org/gen-fac/pubs/astclim/paranal/seeing/singstory.html

solar activity[5] (which strongly affect several sky properties, like night-sky brightness and airglow). The derived main properties have been compared with similar properties at other observatories.

The structure of this article is as follows: in Section 2 we describe the dataset collected for the current study, including a description of data and the data reduction; in Section 3 we show the analysis performed over the different types of data and the results derived for each one; in Section 4 we summarize the main results and present the conclusions.

2. DESCRIPTION OF THE DATA

In order to understand the properties of the night-sky emission at the Calar Alto Observatory we collected different observational data, including both imaging and spectroscopic data. Since none of the data were obtained directly for this study, we scanned thoroughly the arquived data to acquire a data set with a sufficient degree of homogeneity.

2.1. Spectroscopic data

Spectroscopic data were obtained to determine the mean properties of the night-sky spectrum of moonless nights at the observatory. In Calar Alto spectrographs are normally mounted in bright and gray nights, while dark nights are more frequently allocated for deep imaging programs. Thus, it is somehow difficult to find spectrocopic data taken during dark nights. The most frequently mounted spectrographs at the Calar Alto observatory are CAFOS at the 2.2m (∼50% of the allocated time) and PMAS (Roth et al. 2005) at the 3.5m telescope (∼30% of the allocated time). PMAS is an integral field unit with two different setups, a lensarray with a reduced field-of-view ($16'' \times 16''$ in its largest configuration), and a wide fiber-bundle that covers a field-of-view of $72'' \times 64''$ with 331 individual fibers of $2.7''$ diameter each one (PPAK, Kelz et al. 2006). This latter configuration is particularly interesting to study the properties of the sky emission, since in a single shot centred on a calibration star (or a science target) a substantial fraction of the field-of-view samples the sky. Its large aperture, and the possibility of performing self-calibration, allows one to obtain spectrophotometric calibrated and high signal-to-noise spectra of the night-sky emission even with reduced exposure times. Evenmore, this instrument is frequently mounted with a low-resolution grating (V300), which covers a wavelength range of ∼3500Å with a spectral resolution of ∼10Å (FWHM). This is also very convenient to obtain spectra of the sky emission in all the optical wavelength range. Restricting ourselves to the same instrument and configuration ensures the homogeneity of the data.

There were 14 clear moonless nights when the instrument was mounted using this configuration in the period between January 2005 and December 2006. A sample of 23 observations, including night-sky emission spectra, were selected from the data taken that nights. The sample was selected by including only observations of calibration stars and/or small-size and faint targets (eg., High-z Ly-α emitters, Sánchez et al. 2007c), with most of the PPAK field-of-view sampling sky emission. In addition,

only observations near the zenith, with an airmass lower than 1.5, were included in the sample. In all the cases the observations were taken far away the ecliptic and the galactic plane. The data were then reduced using R3D (Sánchez et al. 2006), following the standard steps for fiber-based IFS data. Once reduced, the sky spectra were extracted from the frames using E3D (Sánchez 2004), by selecting areas clean of objects within the field-of-view. Although the signal-to-noise level of each individual sky spectrum is somehow different, depending on the exposure time and the number of selected fibers to extract the spectra, in all the cases is good enough for the purposes of this study.

Not all the observations during a moonless night are equally dark. The darkness of an observation depends strongly on the time distance of the corresponding night from the full moon, the presence of cirrus, dust and local contamination when pointing towards highly populated areas (like Almeria, towards the south of the observatory), the zenith distance, and even more the time distance from the twilight. Thus, from the original dataset we did not consider those spectra which intensity at 5200Å was larger than 0.3 10^{-16} erg s^{-1} cm^{-2} Å^{-1}(V∼20.2 mags). We were then left with a final sample of 10 individual spectra obtained in 7 different nights, representative of the typical dark observation in a moonless dark night at Calar Alto. This sample still comprises a wide range of brightness, and only one (02/06/2005) can be considered completely dark, corresponding to a new moon night. Table 1 shows the final list of nights, together with the wavelength range covered by the spectra each night.

2.2. Imaging data

Multiband imaging data are collected to characterize the sky-brightness of moonless nights at the observatory. The search was restricted to CAFOS covering a similar period of time of the selected spectroscopic dataset, to preserve the homogeneity of the data. Only exposures on calibration fields were selected to perform a self flux-calibration, avoiding the possible errors due to changes in the atmospheric condition between calibration and measurement. Although these exposures tend to have short exposure times, from 20s to 200s, the large field-of-view of CAFOS CCD (∼$15' \times 15'$) and pixel size ($0.53'' \times 0.53''$), allow a good estimation of the sky background. The use of calibration fields, with more than 4 calibration stars observed per field, guarantees a good estimation of the magnitude zero-point per filter and exposure (photometric calibration error <0.1 mags). We focused our search in nights dedicated to a single project, aimed to study the time evolution of the multiband photometry of supernovae (PI: Dr. W. Hillebrandt; Pastorello et al. 2007), observed in service mode. The reason for that was that this program uses the same instrument setup, filters, calibration fields and covers a large periods of time. The number of nights totally or partially dedicated to this project were ∼21 along the considered time period. Finally we selected the darkest possible nights, ie., moonless nights that distance at least 13 days from the full moon. We were then left with 5 nights. However, only in two of them the calibration fields were observed at least one hour after the begining of the astronomical night. In the remaining 3 nights there was still substan-

tial contamination from the twilight, and they are therefore excluded from any further analysis. Table 1 shows the final list of selected nights, including the broad-band filters observed each night.

The Landolt calibration fields PG1633 and PG0918 (Landlot 1992) were observed each night, respectively, in the listed filters. The images were reduced following the standard steps, using IRAF routines. First a master bias frame was created for each night by averaging all the bias frames obtained along the night and smoothing it. All images were then bias corrected by substracting the corresponding master bias. For each band a master flat-field frame was obtained by averaging the bias corrected domeflat images, and normalizing to the median intensity value. Images were then corrected for pixel-to-pixel response variations dividing by their corresponding flat-field frames. No sky subtraction was performed since the aim of this study is to determine its intensity.

2.3. *Extinction data*

The Calar Alto Extinction monitor (CAVEX), is an inhouse developed instrument (PI: U.Thiele), which estimates the monocromatic extinction in the V-band continously along each night. The system is fully automatic, opening half an hour after the beggining of the astronomical night and closing half an hour before its end. It continously points towards the north (the polar star), taking images of $\sim$20s exposure time every $\sim$76s covering a field-of-view of $\sim$55 degrees with a resolution of $2.3'$/pixel. By traking the location of 15-20 stars in the field, it estimates the extinction by measuring their apparent magnitudes across a range of 1.1-2.4 airmasses. It shares the same limits of humidity and wind speed than the telescopes at the obsevatory, producing a measurement of the extinction every $\sim$2 minutes if the night is clear. When the night is cloudy or the extinction has strong fluctuations, the instrument does not produce a reliable data, flagging it. Therefore, the fraction of time without precise extinction measurements from the CAVEX is a good estimation of the amount of time lost due non astronomical weather conditions in the observatory. We have collected all the available data from the extinction monitor during the last 4 years, from May 2003 to May 2007. The data comprises 214193 individual measurements, corresponding to 1044 nights from a total of 1478 nights included in this period.

CAVEX estimates the total extinction in a single band. To characterize the extinction curve it is needed to measure the extinction at different wavelengths. In the Summer of 2006 (27/07/06-15/08/06) and the Winter of 2006-2007 (17/12/06-13/01/07), an instrument built with the sole purpose of estimating this extinction curve was installed, named the Extinction Camera and Luminance Background Register (EXCALIBUR, PI: J.Aceituno). EXCALIBUR is a robotic extinction monitor able to do cuasi-simultaneous photometric observations in 8 narrow bands covering the wavelength range between 3400Å and 10200Å, characterizing the extinction curve in this wavelength range (although only 6 of the bands were operative when installed at Calar Alto). The instrument was built to estimate the aerosol abundance based on the shape of the extinction curve (Pérez-Rámirez 2007a,b). It estimates $\sim$16 extinction coefficients for each of the sampled bands per hour, and an average of $\sim$160 extinction coefficients per band for each night. It was operative for a total of 6 nights in the Summer season and 14 nights in the Winter season. We collected all these data for the current study.

2.4. *Seeing data*

The night-sky seeing is measured by a Differential Image Motion Monitor (DIMM, Aceituno 2004) at the Calar Alto observatory since August 2004, and it is nowadays a fully automatic instrument. It measure the seeing at the wavelengths corresponding to the Johnson V-band. This DIMM was calibrated with a previous one installed in the observatory (Vernin & Muñoz-Tuñon 1995), which, at the same time, was also calibrated with a Generalized Seeing Monitor in May 2002 (Ziad et al. 2005), when they both estimated a median seeing of $0.90''$ for that time period. To study the possible evolution of the seeing at the observatory and its possible dependencies with another night-sky parameters we collected all the available seeing measurements on the time period between January 2005 and December 2006. Contrary to the CAVEX, the DIMM has more severe limitations to be operative, and it closes automatically when the humidity is larger than an 80% or the wind speed is 12 m s^{-1}, which comprises $\sim$50% of the time. The DIMM produces an estimation of the transversal and horizontal seeing in each measurements. Whenever there is an occasional large difference between both estimations (not due to a dominant wind component) they most probably are not due to atmospheric effects, but rather to mechanical oscilations. Due to inherent stability of a DIMM system to this kind of oscilations, these cases comprise a relatively small number ($\sim$5%). They have been excluded from the final dataset. We finally collected a total of 213622 seeing measurements distributed along 335 nights during the considered time period.

3. ANALYSIS AND RESULTS

We describe here the analysis performed over each of the different collected data.

3.1. *Night Sky Spectrum*

The data included in the final sample of night-sky spectra for moonless dark nights described in Section 2.1 were combined to create a typical moonless night-sky spectrum at the observatory. For doing so each spectrum was normalized to the mean intensity (of the sample) at 5200Å (0.13 10^{-16} erg s^{-1} cm^{-2} Å^{-1}). Then the final spectrum was produced by averaging the flux of these normalized spectra at each sampled wavelength. Figure 1 shows the resulting spectrum, covering a wavelength range between 3700 and 7933Å. This is the first time that a typical night-sky spectrum is published for the Calar Alto observatory [6]. The emission lines clearly identified in the spectrum have been labeled with its corresponding atomic name and wavelength. Several of the distinctive features of the night-sky spectrum are due to airglow, although a substantial fraction is due to light-pollution.

The airglow is emitted by atoms and molecules in the upper atmosphere which are excited by solar UV radiation during the day and twilight (Ingham 1972). Airglow

---

[6] The final reduced FITS file can be downloaded from the webpage: http://www.caha.es/sanchez/sky/

is the most important component of the light of night-sky. It produces the 5577Å and 6300Å lines from OI (which are stronger near the twilight). It contributes to the ubiquitious 5890-6Å NaD doublet, although this line is heavily contaminated by light-pollution from low and high preassure street-lamps. Airglow is also responsible for the OH rotation/vibration bands in the red and IR, known as the Meinel bands (Meinel 1950), visible at the redder wavelengths of the spectrum (see Fig. 1). In addition it produces a pseudo-continuum in the blue from overlapping O_2 bands (2600-3800Å) and in the green from NO_2 bands (5000-6000Å). A more detailed description of the effects of the airglow on the night-sky emission can be found in Benn & Ellison (1998a). An atlas of the airglow from 3100Å to 10000Å was presented by Ingham (1962) and Broadfoot & Kendell (1968).

Other contributions to the night-sky spectrum are the zodiacal light, the starlight, and the extragalactic light, which increases the background continuum emission (see Benn & Ellison 1998a and references therein for a more detailed explanation on their effects). All of them, including the airglow, comprises the natural processes that produce the night-sky spectrum in any astronomical site. In addition to them, the night-sky spectrum can be affected by the light-pollution due mostly to the street-lights of populated areas near the observatories. Light pollution arises principally from troposheric scattering of light emitted by sodium and mercury-vapour and incandescent street lamps (McNally 1994; Holmes 1997).

Typical spectra of the three more used types of street-lamps were presented by Osterbrock et al. (1976): the sodium low-pressure lamps, the sodium high-pressure lamps and the mercury lamps. The first of the three is the one with less impact in astronomical observations, since its produces most of its light concentrated in the 5890-6Å NaD and 8183-95Å NaD emission lines. Therefore only a very reduced number of astronomical observations are strongly affected by them. On the other hand the high-pressure sodium lamps emitt most of its light in a broad NaD line centred in ~5890Å, with a FWHM of ~400Å, that shows a central reversal. They also show a strong 8183-95Å emission line, and fainter emission lines at 4494-8Å, 4665-9Å, 4758-52Å, 4979-83Å, 5149-53Å, 5683-88Å, 6154-61Å and 7665,7699Å. The high-pressure sodium lamps may affect strongly the quality of any astronomical observation. Finally the mercury lamps produce narrow lines at 3651/63Å, 4047Å, 4358Å, 5461Å, 5770Å and 5791Å, together with broad features at 6200Å and 7200Å of FWHM~100Å, from the phosphor used to convert UV to visible light. They also produce a weak continuum emission over the whole visible range. Some mercury pollution lines can strongly affect certain astronomical studies: (i) the 4358Å Hg line strongly affect any attempt to measure the emission of the 4364Å [OIII] line in any object in the Galaxy. This line is fundamental for the estimation of the electron temperature of galactic nebulae. (ii) the 5460Å Hg line lies in the centre of the y-band of the $ubvy$ Strömgren photometric system, which may affect the programs devoted to the study of stellar populations that use this filter set.

Other sources of light pollution are the incandescent lamps and the high-pressure metal halide lamps. The spectrum of the former consists of continuum emission only, and it is difficult to identify in a night-spectrum. The latter are nowadays frequently used in the illumination of sport stadiums and arquitectonical monuments (which can be considerable, since they are normally oriented towards the sky). These high-pressure metal halide lamps exhibit some Scandium, Titanium and Litium emission lines, that are charactezed by a blue edge due to molecular bands (General Electric 1975; Lane & Garrison 1978; Osterbrock et al. 1976).

The night-sky spectrum shown in Fig.1 shows clear evidence of strong light pollution from all the street-lamps described before. It shows strong Mercury lines all over the spectrum, the typical emission lines and features of high-pressure sodium lamps, with a well detected broad emission at ~5900Å, and a strong NaI emission line at 5893Å indicative of low-pressure sodium lamps. Evenmore, it also presents the typical emission lines corresponding to high-pressure metal halide lamps. All this pollution comes from the populations nearby the observatory, in particular from Almeria (~250000 habitants), at 40 km towards the south, and smaller towns at the north (like Baza, ~21000 habitants, and Macael, ~6000 habitants). There are well established estimations of the contribution of city lighting to dark-sky brightness (e.g., Treanor 1973, Walker 1973, Yocke et al. 1986, Garstang 1991, and reference therein). However, its contribution to the spectrum is more complex, since it depends on the particular kind of lamps used for street illumination. Most major observatories nearby populated areas have some kind of night-sky protection laws with the aim of reducing the effects of light pollution by controlling the fraction of light that escapes towards the sky and the kind of lamps used (normally they promote the use of low-pressure sodium lamps). The Calar Alto Observatory does not benefit yet from any local sky-protection law which regulates the street illumination, with the corresponding effects that can be appreciated in the night-sky spectrum.

To estimate the contribution of light pollution to the night-sky spectrum we derive the flux intensity corresponding to each of the detected emission lines. Each line was fitted with a single gaussian function using FIT3D (Sánchez et al. 2007a), using the same procedure described in (Sánchez et al. 2007b). Table 2 lists the integrated flux for each of the detected emission lines shown in Fig.1, together with the identification of the line and the nominal wavelength. In addition to the emission lines, the flux intensity of the sodium broadband emission at ~5900Å was also estimated by fitting the feature with a single broad gaussian function. The result is also listed in Table 2. All the fluxes were converted to Rayleighs following the conversion formulae by Benn & Ellison (1998a).

These values can be compared to those ones obtained for another astronomical sites. E.g., Pedani (2005) presented a study of the night-sky spectrum at the Observatory of the Roque de los Muchachos, La Palma. The intensity of the lines produced by the Mercury and low-pressure Sodium lamps found in our spectrum are only comparable to those ones in La Palma when pointing in the directions towards the most polluting towns in this island. On the other hand, the contribution of the lines produced by the high-pressure Sodium lamps is much lower, being comparable to that of the less polluted ar-

eas of the sky in La Palma. This may indicate that most of the street lamps used in Almeria are Mercury and low-pressure Sodium lamps, rather than high-pressure Sodium ones, and therefore they only affect specific wavelength ranges (and science programs). Finally we clearly see lines produced by high pressure metal halide lamps, only marginally (and recently) detected in the sky spectrum at La Palma (Pedani 2005).

Once determined the contribution of each emission line to the night-sky spectrum it is possible to decontaminate it by the effect of the pollution lines (ie., all but the OI ones), creating a *clean* night-sky spectrum. This can be done directly for the Mercury, Scandium, Titanium and Litium lines, since all its emission is produced by light pollution. However, in the case of the Sodium lines there is a natural contribution due to the airglow. We lack a direct measurement of this natural contribution at Calar Alto, that can only be achived nowadays with a general blackout. However its natural contribution must not be significantly larger than in other astronomical sites. Benn & Ellison (1998a) estimated the natural contribution by the broad Sodium emission band in ∼0.03 mag in V and ∼0.02 mag in R for La Palma observatory. Similar contributions are expected by the NaI 5893,6 emission lines. Therefore, the natural contribution by the Sodium due to the airglow is expected to be of the order of ∼0.04 mag in both bands. Thus, as a first order we can assume that all the detected emission by Sodium in our sky-emission spectrum is due to pollution, and once determined its contribution we can correct it by the expected contribution of natural emission, if needed.

Table 3 lists the estimated contribution of the light pollution to the sky background in different bands. It includes the B, V and R-Johnson filters, and a set of medium band filters selected from those ones used by the ALHAMBRA survey (Moles et al. 2007), a major imaging survey currently on going at the Calar Alto observatory. They are included to illustrate the effects of the pollution lines in the background sky when using median/narrow-band filters affected by these lines. The contamination from light pollution is clearly stronger in the B-band than in other astronomical sites: e.g, ∼0.02 mag at La Palma (Benn & Ellison 1998a), 0.02-0.04 mag at Kitt Peak (Massey et al. 1990). Although there are astronomical sites with similar or stronger contaminations: e.g. Mount Hopkins (see Fig. 2, from Massey & Foltz 2000). This contamination can be reduced by a proper light pollution law that limits the use of the Mercury street lamps. Strong benefits from such laws has been experienced in different sites (e.g., Benn & Ellison 1998a; Massey & Foltz 2000). The contamination in the V and R-bands is slightly stronger than in some other places, like La Palma: 0.05-0.10 mag at the V-band and 0.07-0.12 mag at the R-band (Pedani et al. 2005), but it is similar or smaller than in other astronomical sites, like Kitt Peak: 0.19-0.33 mag in the V-band (Massey et al. 1990) or Mount Hopkings: 0.17 mag in the V-band (Massey & Foltz 2000). One of the two recomendations of the IAU for a dark place is that the contribution of the pollution to the Sodium emission should not exceed in intensity the natural airglow one (Smith 1979). If we consider that the airglow emission is similar in Calar Alto than in La Palma (or at least of the same order), it is clear that the contribution from the light pollution

is much stronger. In these regards Calar Alto does not fulfill the IAU recomendations for a dark place. A proper light-pollution law, that increases the use of low-preasure sodium lamps rather than high-presure ones, will not reduce the net effect of the light pollution to the sky-background in these bands, but it will concentrate it in a more reduced wavelength range, affecting less observing programs.

Most of the lamps that cause the light pollution also produce a certain level of continuum emission. In particular Mercury and high pressure metal halide ones. However its contribution is difficult to estimate. Although we donecannot quantify its effect, the reduction of the use of Mercury, high-pressure Sodium lamps and high pressure metal halide lamps in the vicinity of the observatory will certainly also reduce the sky-background continuum.

The lack of previous similar studies of the night sky spectrum at the Calar Alto observatory (to our knowledge) does not let us to analyze the evolution of the light pollution along the time.

3.2. *Night Sky Brightness*

The night sky brightness was determined by using both the imaging and spectrocopic data described before. In the case of the imaging data, the calibration fields contain at least 5 calibration starts per frame. The magnitude zeropoint for each image was determined by measuring the counts intensity of each of these stars within a fixed aperture of $8''$ radius, using IMEXAM task of IRAF package, and applying the formula:

$$mag_{zero} = mag_{app} + ext + 2.5\log_{10}(counts/t_{exp})$$

where mag_{zero} is the magnitude zeropoint, mag_{app} is the apparent magnitude of the calibration star in the corresponding band, ext is the extinction, derived from the correponding value measured by the CAVEX this night and the airmass of the image, $counts$ are the measured counts within the indicated aperture, and t_{exp} is the exposure time. Since the measured seeing of the images (FWHM of the field stars), ranges between $0.9''$ and $1.3''$, this aperture ensures that most of the flux is contained within it, and no aperture correction was applied. The average of the values derived for each calibration star in the field is considered the zeropoint of the image, and the standard deviation from this mean value is considered as the photometric error. This standard deviation ranges between 0.02 mag and 0.06 mag for each band and each night.

The sky brightness was then determined in each image by measuring the mean counts level in several (> 10) square apertures of $\sim 50'' \times 50''$, in areas free of targets, using IMEXAM task of IRAF package. The mean value of these measurements is considered as the count level of the sky brightness, and the standard deviation with respect to this mean value the error in the count level estimation. Finally, the sky surface brightness was determined using the formula:

$$SB_{sky} = mag_{zero} - 2.5\log_{10}(counts_{sky}/t_{exp}/scale^2)$$

where SB_{sky} is the surface brightness in magnitudes per square arcsec, mag_{zero} is the zeropoint described before, $counts_{sky}$ is the sky counts level estimated and *scale*

is the pixel scale in arcseconds (ie., 0.53″ for CAFOS). It is noticed that the magnitude zeropoint was corrected by the extinction, but the sky brightness was not, following the convention adopted in most of the recent studies of sky brightness (e.g., Walker 1988b; Krisciunas 1990; Lockwood et al 1990; Leinert et al. 1995; Mattila et al. 1996; Benn & Ellison 1998a,b). Correcting the sky brightness for extinction would be appropiate only if the extinguishing layer were known to be below all sources of sky brightness, which is not the case (Benn & Ellison 1998a,b).

In addition to the estimations of the sky surface brightness obtained using direct imaging we also derived the sky surface brightness by using the PPAK spectroscopic information for the only full moonless night of our sample (02/06/2005). The two night-sky spectra obtained this night cover the wavelength range of the B, V and R-band filters. We derived the sky flux intensity for each of these filters by convolving each spectrum with the corresponding filter tranmission curves listed in the Asiago Database on Photometric Systems (Moro & Manuri 2000). Then the fluxes were transformed to magnitudes by using the zero-pointings listed in Fukugita et al. (1995). The mean value of the two derived magnitudes in each filter is adopted as the sky surface brightness of that night, and the absolute difference between both magnitudes as the error.

Table 4 lists the sky-surface brightness obtained from both the imaging and spectroscopic data at the different bands for each moonless night. In addition, it lists previous results on the sky-brightness at different astronomical sites, including the results presented by Leinert et al. (1995) for Calar Alto, derived from broad-band photometry obtained along three nights in 1990.

Dependency on the zenith distance

There is a wide range of sky surface brightness values for the different bands, considering that all the measurements were obtained in full moonless nights, without twilight contamination. The data from the first night, derived using PPAK data, are very similar to those ones from the third night, derived using CAFOS data, being the sky in the former slightly brigher in the B-band. The sky brightness of the second night is brighter in all the bands. Looking back to the data, we realize that the airmass of the images of the 1st night ($\sim$1.7), corresponds to an eleveon much lower than that of the 2nd and 3rd night data ($\sim$1.3 and $\sim$1.2, respectively). The sky brightness increases with the airmass for two different reasons. One is a natural effect of the airglow, which is brighter at low elevations cause the line of sight intercepts a larger number of atoms in the airglow layer (Garstang 1989; Benn & Ellison 1998a, and references therein). A second effect is the increase of light pollution when pointing towards high populated areas at low airmass. Walker (1971,1991) and Garstang (1989) estimate that the increase in the brightness at an air mass of $\sim$1.4, in the direction of a populated area of P inhabitants at a distance D km to be $\sim \frac{PD^{-2.5}}{70}$ mag. That would correspond to $\sim$0.3 mag when pointing directly towards the south, where is the largest populated city nearby (Almeria). However since our observed fields are mostly pointing towards the east its contribution is more

difficult to estimate. It is not possible to know which is the actual contribution of the light pollution to the continuum brightness at the zenith. Therefore we do not know if Calar Alto fulfill (or not) the other IAU recomendation for a dark site, that is that this contribution must be lower than $\sim$0.1 mag (Smith 1979).

It is possible to derive an approximate expression of the sky brightness dependecy on the zenith distance due to natural effects based on the results by Garstang (1989), as already pointed out by Krisciunas & Schaefer (1991). This expression can be used to correct the measured values and derive a much appropiate estimation of the zenithal sky brightness (Benn & Ellison 1998a; Patat 2003). Patat (2003) derive the following formula (Appendix C of that article) for this correction:

$$\Delta m = -2.5\log_{10}[(1-f) + fX] + \kappa(X-1)$$

where Δm is the increase in sky brightness at a certain band and airmass (X), f is the fraction of the total sky brightness generated by airglow, being (1-f) the fraction produced outside the atmosphere (hence including zodiacal light, faint stars and galaxies) and κ is the extinction coefficient at the corresponding wavelength.

We applied this correction to our data, using the typical extinction curve at Calar Alto (following sections) normalized to the corresponding κ_V extinction coefficient of each night. A typical value of f =0.6 was used for this correction (Patat 2003). Once applied there is a significant reduction of the dispersion between the values obtained for each night. This indicates that the correction works pretty well, despite the fact that it does not take into account the effects of light pollution. The mean values of the sky brightness at the zenit after correction for each band are also listed in Table 4.

Variation of the sky-brightness along the time

The night sky-brightness at Calar Alto shows no significant change in the last 15 years, when comparing with the results by Leinert et al. (1995). They did not applied any correction for the dependecy on the zenith distance to their data (Table 6 of that article). Therefore we must compare with the mean values without correction. The only band where it is appreciated an increase of the sky-brightness is the U-band ($\sim$0.4 mag brigther). However, if we take into account that we only have data for this band at low elevation, we cannot consider these results conclusive. For the remaining bands the sky seems to be $\sim$0.2 mag brighter in the B-band, $\sim$0.2 mag fainter in the R-band and without changes in the V- and I-bands, when comparing with the mean values derived for the three nights of our sample. However none of these differences seems to be significative, lying withing the errors of our measurements. When comparing with the two darkest nights with data obtained at high elevation the differences (if any) disappear for the B and V-bands, and the sky seems to be even darker in the R and I-band. A possible caveat to this comparison is that the results listed in Leinert et al. (1995) were obtained not exactly in the solar minimun, which may produce an increase of the sky-brightness. However, although their broad-band data were obtained in the 1990, they also obtained intermediate-band data in the 1993 and their sinthetized

broad-band surface sky-brightness are similar to those obtained in the nights of the 1990.

Comparison with other astronomical sites

The sky surface brightnesses at the Calar Alto observatory at different bands, listed in Table 4, are remarkable similar to those ones at many other different astronomical sites. In the optical wavelength range (U,B,V and R-bands), Calar Alto seems to be a particular dark site, comparible to Mauna Kea. The fact that both places seem darker than Paranal may be an artifact since the data presented by Patat et al. (2003) were taken during the maximun of solar activity. This result is in anycase remarkable, considering the strong light pollution present in the Calar Alto spectra, which effect is particularly strong in the B, V and R-bands (Tab. 3). Most of the listed observatories have little light pollution or they benefit of specific protection laws against it. This has been demonstrated as a tremendous useful tool to preserve or increase the quality of the night-sky (eg., Benn & Ellison 1998a,b; Massey & Foltz 2000; Walker & Schwarz 2007). If the effects of light pollution could be reduced in the vicinity of Calar Alto it would become a particularly dark site for optical observations.

On the other hand, the sky is clearly brighter in the I-band than in any other astronomical site listed in this table. Despite the fact that the observatory is located in the most arid place in Europe, in the vecinity of a desert (the Tabernas desert), the water vapor Meinel bands are particularly strong. The humidity at Calar Alto is higher than in other astronomical sites, like Paranal or Mauna Kea, although there are frequent epochs of low humidity (<20%) in the Summer. The height of the observatory, $\sim$2200 m over the sea level, normally places it under the inversion layer, which has a particular strong impact in the strength of the water vapor emission lines. Both combined effects can explain the rise of the sky-brightness in the I-band. It is important to note here that this effect has a relatively reduced effect over near-infrared observations in the J, H and K-band.

3.3. Extinction coeffcients

The median V-band extinction at the Calar Alto observatory for the time period covered by the CAVEX data (Section 2.3) was $\sim$0.18 mag, with a mean value of $\sim$0.21$\pm$0.08 mag. This value is slightly smaller than the previously reported by Hopp & Fernandez (2002), which was based on a much smaller sample of data (comprising 74 nights spanned between 1986 and 2000). They found that there was an increase of the extinction at the Summer season, that was most probably associated with an increase of the aerosols (ie. dust) in this period of the year. Similar seasonal pattern has been appreciated in another major observatories: e.g., La Palma observatory is strongly affected by dust extinction in the Summer when dust from the Sahara desert ($\sim$400 km away) blows over the Canary Islands (Benn & Ellison 1998a). Although the Calar Alto observatory is nearer to the Sahara desert ($\sim$250 km away) than La Palma, it is normally out of its main wind streams, being shielded by the Altas mountains. On the other hand, it is located in an arid region nearby a much smaller desert, the Tabernas desert ($\sim$15 km away).

Figure 2 shows the evolution of the average V-band extinction for each night along the period of time sampled by the dataset. As already suspected by Hopp & Fernandez (2002), there is a clear seasonal pattern. The typical extinction in the Winter nights is $\kappa_V \sim$0.15 mag, being mostly restricted to values lower than $\kappa_V <$0.2 mag. In Summer time there is a wider range of extinctions, although in most of the cases the extinction is lower than $\kappa_V <$0.4 mag. As indicated before this increase of the extinction is most probably associated with a rise of the aerosols (dust) in the atmosphere. We will explore that possibility latter.

This seasonal pattern is somehow similar to the one seen in La Palma. Indeed the fraction of nights with $\kappa_V >$0.25 mag is similar in both observatories, $\sim$20% of the nights. However there is a major difference: the fraction of nights with high extinction, $\kappa_V >$0.4 mag, at Calar Alto is very reduced, $\sim$3%, while at La Palma this fraction is $\sim$10% of the nights, with frequent peaks of extinction over $\kappa_V >$0.6 mag (Benn & Ellison 1998a, Figure 3).

Based on the fraction of nights that the CAVEX was operative and derived realiable measurements of the V-band extinction (κ_V), it is estimated that $\sim$70% of the nights were astronomically useful in the period covered by these data (4 complete years). This fraction is remarkable similar to that one in many other astronomical sites (eg., La Palma, Benn & Ellison 1998a). The fraction of fully photometric nights, defined as nights where the V-band extinction varies less than a 20% along all the night, was $\sim$30%.

Contributions to the extinction

The EXCALIBUR data described in Section 2.3 were used to determine the typical extinction curve at Calar Alto. This curve was previously studied by Hopp & Fernandez (2002), using an inhomogenous dataset. The extinction coefficients were analyzed separately for the Summer and Winter seasons due to the observed seasonal pattern. First, it was derived the mean extinction coefficients per night by averaging all the measured extinction coefficients per band obtained along each night ($\sim$160 values). Then, the mean extinction coefficients per season were determined by averaging all the measured extinction coefficients per band obtained along each season nights. Table 5 lists the average extinctions coefficients obtained for each season for each of the 6 bands sampled by the instrument, including their central wavelengths and the standard deviation with respect to these mean values. As expected the standard deviation in the extinction coefficients is larger for the Summer data than for the Winter ones, in agreement with the results shown in the previous section. The EXCALIBUR results are consistent with the CAVEX ones for the wavelength covered by both instruments, ie., $\sim$500 nm. This indicates that the extinction coefficients listed in Table 5 are a good representation of the typical values for each season.

The total extinction is mostly due to three contributions, the Rayleigh scattering at the atmospheric atoms and molecules, the extinction due to aerosol particles (mostly dust), and extinction due to Ozone (Walker 1987b). The Rayleigh scattering can be described by

$$\kappa_{RC} = B(p, t, n')\lambda^{-4}$$

where λ is the wavelength and B is a constant that mostly depends on the pressure, the temperature and the normalized refractive index of the air (n', slightly wavelength dependent). In general B can be replaced by its average value for the mean conditions in a certain astronomical site (e.g., Rufener 1986). The aerosol particles produce a similar absorption, that can be described by

$$\kappa_p = b(h_{obs})\lambda^{-\alpha}$$

where b is a parameter that depends mostly on the height of the observatory (h_{obs}), and α is a power law index that depends on the size of the aerosol grains. Although an $\alpha \sim 1.3$, derived by Siedentopf (1948), is widely used, we adopted a value of $\alpha =0.8$ for consistency with the previous study of the extinction curve at Calar Alto (Hopp & Fernandez 2002). The Ozone extinction is a selective absorption by molecular bands. It can be approximately described by a broad gaussian function centred in $\lambda \sim 6000$ Å (matching the shape shown in Runefer 1986 and Hopp & Fernandez 2002):

$$\kappa_{O3} = C \exp[-\frac{\lambda - 6000}{1200}]$$

Each single contribution to the extinction depends on the wavelength and a particular constant that, in the case of the two first, depends on the height and the average atmospheric conditions in the observatory. We adopted the values listed for $\lambda =5400$Å in Rufener (1986), consitent with those derived by Tüg (1977), obtained for La Silla observatory. A similar approach was followed by Hopp & Fernandez (2002). The height and average weather conditions in this observatory are very similar to those of Calar Alto, which justifies the use of these constants.

Therefore the total extinction curve is a linear combination of these three contributions:

$$\kappa_\lambda = f_1 \, \kappa_{RC} + f_2 \, \kappa_p + f_3 \, \kappa_{O3}$$

The extinction coefficients for the two seasons were fitted to this linear combination, deriving the relative contribution of each one (f_i) to the total extinction. Table 6 lists the results from this fitting analysis, including the relative contribution (f_i) derived for each component for each season. For comparison it also includes the same relative contributions derived for Calar Alto by Hopp & Fernandez (2002), and their compilation of similar results for different astronomical sites.

The contribution of the Rayleigh scattering seems to be rather constant for the two considered seasons, like the Ozone absorption. On the other hand, the Aerosol contribution rises considerable in the Summer time, being responsible of the increase of the extinction in this season, as it was thought. The estimated contributions of the Rayleigh scattering and the Aerosol extinction are very similar to the values reported by Hopp & Fernandez (2002) for the Winter season, which may indicate that both contributions have not changed considerably with time (their data corresponds to 1986-2000). Both contributions are also similar to the ones derived for other major astronomical sites. On the other hand the contribution of the Ozone absorption seems to be stronger

than in previous measurements and other astronomical sites. Unfortunaly the coverage of EXCALIBUR when mounted at Calar Alto did not allow to perform an accurate sampling of the wavelength range affected more strongly by the Ozone absorption, which did not let us to be conclusive on this respect.

Figure 3 shows the distribution of the extinction coefficients along the wavelength for the two season datasets. It also includes the best fitted linear combination of the three components to the extinction and each of these components scaled to its relative contribution to the total extinction. Despite the apparent increase of the Ozone absorption its actual contribution to the total extinction at any wavelength is very limited, being neglectible in comparison with the other two contributions. Indeed the fitting process derives equally good results when this contribution is removed. As already indicated the Rayleigh scattering contribution is very similar for both datasets, being the dominant contribution in the Winter season, ie., in conditions of low extinction. In Winter time is responsible of the $\sim 85\%$ of the extinction in the V-band, only $\sim 11\%$ is due to Aerosol extinction and $\sim 4\%$ to Ozone absorption. On the other hand, in Summer its contributions drops to $\sim 63\%$, with $\sim 35\%$ due to Aerosol extinction and $\sim 2\%$ due to Ozone absorption. Curiously, the contribution of Aerosols to the extinction in the conditions of minimun extinction are much reduced than the one found in other astronomical sites, like La Silla (Burki et al. 1995).

The Extinction Curve

As we shown in the previous section the extinction curve depends strongly on the relative contribution of each of the three major components to the extinction. Each of them has a different dependecy with the wavelength, and two of them depends also on the particular atmospheric conditions at the observatory. Therefore, it is difficult to derive a precise extinction curve valid for every night that depends only in a reduced number of parameters. However it is still possible to look for an approximate expression for the extinction curve that provide an useful estimation of the extinction at any wavelength and that depends only in a single parameter: the V-band extinction, measured each night by the CAVEX.

Based on the results of the previous section it is known that the Ozone absorption have a marginal effect in the total extintion at any wavelength. Therefore we have not considered it for our approximate expression. It is also known that the contribution of the Rayleigh scattering is almost contant along the year, and therefore the variations in the extinction are controlled by the amount of Aerosol particles (ie., dust). Based on this assumption an approximate expression for the extinction curve can be derived by considering that the extinction in the V-band is due to a fix contribution of Rayleigh scattering (the average for both seasons) and a variable contribution due to Aerosol extinction. The derived expression is:

$$\kappa_\lambda \sim 0.0935 \left(\frac{\lambda}{5450}\right)^{-4} + (0.8*\kappa_V - 0.0935)\left(\frac{\lambda}{5450}\right)^{-0.8}$$

The typical differences found in the extinction coefficients derived using this formula and the more precise

decomposition presented in the previous section are of the order of ~10%.

3.4. *Atmospheric Seeing*

The seeing data described in section 2.4 were used to determine an average seeing for each night comprised in the dataset (spanned along ~2 years). The median atmospheric seeing for all the time period was ~0.90″, with a ~70% of the nights under subarcsecond seeing (<1″). Figure 4 shows the nightly averaged seeing distribution along the time. The epochs without data in April 2005 and March 2006 were due to reparations in the hut of the DIMM. There is a mild seasonal pattern in the seeing distribution, with the best seeing concentrated in the Summer season. To further investigate this possibility we created the seeing histogram for all the data comprised in the dataset and for two different subsets of data corresponding to the Summer season (May-September) and the Winter season (the rest of the months). Figure 5 shows the three histograms. The differences in the seeing distribution for the Summer (median seeing ~0.87″) and the Winter seasons (median seeing ~0.96″) are clearly appreciated. Not only the median seeing is better in the Summer season, the chances of having better seeing in a Summer night are larger.

Table 7 lists the median seeing estimated for both the total sample and the two season subsamples. For comparison purposes it also lists the atmospheric seeing measured at different astronomical sites world-wide, ordered by increasing seeing. Although the median seeing at Calar Alto is larger than that of some major astronomical observatories (Mauna Kea, La Palma), it is actually better than in many other astronomical sites (eg., Mt-Graham, Paranal).

4. CONCLUSIONS

We have characterized the main properties of the night-sky at the Calar Alto observatory, comparing them, when possible, with similar properties of other different astronomical sites. The main results of this article can be summarized in the following points:

- An average night-sky spectrum for the moonless dark-time at the observatory has been presented for the first time. This spectrum, which covers the optical wavelength range (3700-7933Å), is distributed freely to the community. Airglow and light-pollution emission lines are detected in this spectrum. The strength of the light-pollution lines has been measured, estimating their contribution to the emission in different bands. In comparison with other sites the Mercury lines are particularly strong. The contribution of the light pollution to the Sodium emission is far stronger than its natural emission. In this regards Calar Alto does not fulfill the IAU recomendations for a dark astronomical site (Smith 1979), like other major astronomical sites (eg., La Palma, Pedani 2005).

- The moonless night-sky brightness at the zenith has been determined for the U, B, V, R and I-bands. There was no appreciable change in the sky-brightness over the last 15 years. In comparison with other astronomical sites, Calar Alto shows a particularly dark sky in the optical bands, similar to that of MtGraham or Mauna Kea. The sky brightness could be even darker if it was possible to reduce the light pollution in the optical bands, which would place Calar Alto as a very dark astronomical site. On the other hand, the sky is brighter in the I-band, mostly due to the strength of the water-vapor Meinel bands.

- The extinction, measured along the last 4 years, shows a seasonal dependency with a typical value of k_V ~0.15 mag in Winter time and a wide range of values in Summer, most of them restricted to k_V <0.4 mag. This seasonal pattern, caused by Saharan dust, is similar to the one found in La Palma, but with a smaller range of values in Summer time. The analysis of the typical extinction coefficients at different wavelenghts for each season indicates that the rise of the extinction in Summer is due to an increase of Aerosols (dust) in this period of the year. Due to the reduced contribution of the Ozone absorption to the extinction, and the stability of the contribution of the Rayleigh scattering along the year it was possible to derive an aproximate expression for the extinction curve parametrized only by the V-band extinction.

- The fraction of astronomical useful nights, when the weather was good enough to allow an acurate measurement of the extinction, was ~70% of the nights in the last 4 years. This fraction is similar to the one found in La Palma (Benn & Ellison 1998). The fraction of these nights that were photometric was a ~30%.

- The median seeing along the last 2 years was 0.90″, being slightly better in Summer (0.87″) than in Winter (0.96″). The seeing was better than 1″ in a ~70% of the nights. Although this seeing is slightly worse than in some astronomical sites (eg. Mauna Kea, La Palma), it is better than the currently seeing at Paranal or MtGraham, two astronomical sites where 10m-like telescope are currently in operation or under construction.

We conclude that Calar Alto remains a good astronomical site, similar in many aspects to places where there are 10m-like telescopes under operation or construction. It will strongly benefit from a sky protection law that would reduce the light pollution, particularly due to Mercury and high-pressure Sodium street lamps. Such a law has been under discussion by the local Andalusian goverment during the last few years and we hope it will be soon operative.

The fact that Calar Alto is placed in continental Europe is a major advantage in comparison with other European observatories away from the continent, since both the operational and development costs are significantly smaller.

For both reasons we consider that this observatory is a good candidate for the location of future large aperture optical telescopes.

REFERENCES

Aceituno, J., 2004, Calar Alto Newsletter n.8, http://www.caha.es/newsletter/news04b/Aceituno/Newsletter.html
Benn, C.R., Ellison, S.L., 1998, La Palma Techincal Note, 115.
Benn, C. R., & Ellison, S. L. 1998, New Astronomy Review, 42, 503
Broadfoot, A.L., & Kendall, K.R., 1968, J. Geophys. Res., 73, 426
Burki, G., Rufener, F., Burnet, M., Richard, C., Blecha, A., & Bratschi, P. 1995, A&AS, 112, 383
Fukugita, M., Shimasaku, K., & Ichikawa, T. 1995, PASP, 107, 945
Garstang, R. H. 1989, PASP, 101, 306
Garstang, R.H., 1991, PASP, 103, 1109
General Electric Co. 1975, *High Intensity Discharge Lamps*, Booklet TP-109R
Holmes, R.W., 1997, Observatory, 117, 25
Hopp, U., Fernández M., 2002, Calar Alto Newsletter n.4, http://www.caha.es/newsletter/news02a/hopp/paper.pdf
Ingham M.F, 1962, MNRAS, 124, 505
Ingham M.F, Sc. American, Jan. 1972, p.78
Kelz, A., Verheijen, M.A.W., Roth, M.M. et al., 2006, PASP, 118, 129
Krisciunas, K., 1990, PASP, 102, 1052
Krisciunas, K. 1997, PASP, 109, 1181
Krisciunas, K., & Schaefer, B. E. 1991, PASP, 103, 1033
Landolt, A.U., 1992, AJ, 104, 340
Lane, M. C., & Garrison, R. F. 1978, JRASC, 72, 198
Leinert, C., Vaisanen, P., Mattila, K., & Lehtinen, K. 1995, A&AS, 112, 99
Lockwood, G.W., Floyd, R.D., Thompson, D.T., 1990, PASP, 102, 481
Massey, P., Gronwall, C., Pilachowski, C.A., 1990, PASP, 102, 1046
Massey, P., Foltz, C.B., 2000, PASP, 112, 566
Massey, P., Abraham, T., Bohannan, B., Claver, C., Green, R., Jacoby, G., Wolff, R., 2000, NOAO Newsletter, KPNO Operations, March 2000, Number 61
Mattila K., Väisänen P., v. Appen-Schuur G.F.O., 1996, AAS, 119, 153
McNally, D., 1994, ed. 'The Vanishing Universe - Adverse Entironmental Impacts on Astronomy' (Cambridge University Press 1994).
Meinel, A.B., 1950, ApJ, 111, 433
Moles et al., 2007, AJ, submitted
Moro, D., & Munari, U. 2000, A&AS, 147, 361
Muñoz-Tuñon, C., Vernin, J., & Varela, A. M. 1997, A&AS, 125, 183
Osterbrock, D. E., Walker, M. F., & Koski, A. T. 1976, PASP, 88, 349

Pastorello, A., et al. 2007, MNRAS, 376, 1301
Patat, F. 2003, A&A, 400, 1183
Pedani, M., 2005, The ING Newsletter, 9, 28
Pérez-Rámirez, D., Aceituno, J., Ruiz, B., Olmo, F.J. and Alados-Arboledas, L., 2007, Atmospheric enviroment, accepted.
Pérez-Rámirez, D., Ruiz, B., Aceituno, J., Olmo, F.J., & Alados-Arboledas, L., 2007. "Application of sun/star photometry to derive the aerosol optical depth". International Journal of Remote Sensing. In press.
Pilachowski, C. A., Africano, J. L., Goodrich, B. D., & Binkert, W. S. 1989, PASP, 101, 707
Racine, R. 1989, PASP, 101, 436
Roth, M.M., Kelz, A., Fechner, T., et al., 2005, PASP, 117, 620
Rufener, F. 1986, A&A, 165, 275
Sánchez, S. F. 2004, AN, 325, 167
Sánchez, S. F. 2006, AN, 327, 850
Sánchez S.F., García-Lorenzo, B., Pecontal-Rousset, A., 2007a, Proceedings of the XIII IAC Winter School, Arribas, S., Mediavilla, E., & Roth, M., Ed., in press.
Sánchez, S. F., Cardiel, N., Verheijen, M. A. W., Martín-Gordón, D., Vilchez, J. M., & Alves, J. 2007b, A&A, 465, 207
Sánchez, S. F. et al., 2007c, in prep.
Siedentopf, H., 1948, Naturwiss. 35, 289
Smith, F.G., 1979, Trans IAU, 17A, 220
Taylor, V. A., Jansen, R. A., & Windhorst, R. A. 2004, PASP, 116, 762
Treanor P.J., 1973, Observatory, 93, 117
Tüg, H., 1977, Messenger, 11, 7
Vernin, J., & Muñoz-Tuñon, C. 1995, PASP, 107, 265
Walker M.F., 1971, PASP, 83, 401
Walker M.F., 1973, PASP, 85, 508
Walker, A., 1987a, NOAO Newsletter, No. 10, 16
Walker, A., 1988a, NOAO Newsletter, No. 13, 22
Walker G., 1987b, Astronomical Observations, Cambridge Uni. Press, p. 47ff
Walker M.F., 1988b, PASP, 100, 496
Walker M.F., 1991, in 'Light Pollution, Radio Interference and Space Debris', ed. D.L. Crawford, PASP conference vol. 17, p.52
Walker, A., Schwarz, H.E., 2007, *http://www.ctio.noao.edu/site/pachon_sky/*
Yocke, M.A., Hogo, H., Henderson, D., 1986, PASP, 98,889
Ziad, A., et al. 2005, MNRAS, 362, 455

TABLE 1
LOG OF THE DATA-SET PER NIGHT

Date	Instrument	wavelegth range
25/05/05	PPAK	3700-7000Å
26/05/05	PPAK	3700-7000Å
02/06/05	PPAK	3700-6800Å
30/06/05	PPAK	4700-7940Å
03/07/05	PPAK	3700-7100Å
05/07/05	PPAK	3700-7100Å
23/08/06	PPAK	3700-7000Å
Date	Instrument	Filter Bands
28/08/05	CAFOS	U,B,V,R & I-bands
28/03/06	CAFOS	B,V,R & I-bands

TABLE 2
PROPERTIES OF THE DETECTED EMISSION LINES

Line Id	Wavelength (Å)	Flux*	Flux** R
HgI	4047	3.5	9.6
HgI	4078	0.7	2.0
NaI	4165,8	1.2	3.6
HgI	4358	6.7	22.9
NaI	4420,3	0.3	1.1
TiI	4511.6	3.6	13.7
NaI	4665,9	1.4	5.9
HgI	4827,32	0.5	2.3
NaI	4978,83	1.5	7.7
NaI	5149,53	0.5	2.8
NI	5199	0.7	4.1
ScI	5351.1	3.0	19.0
HgI	5461	6.4	43.1
OI	5577	32.7	234.5
NaI	5683,88	2.9	22.0
HgI	5770,91	5.0	39.7
NaI	5893,6	4.0	33.8
Broad NaD	5893	14.9	126.0
NaI	6154,61	0.9	8.7
OI	6300	18.5	191.2
OI	6364	6.5	69.3
Li	6708	0.3	3.7

∗ in units of 10^{-16} erg s^{-1} cm^{-2}
∗∗ in units of rayleighs.

TABLE 3
CONTRIBUTION OF THE LIGHT POLLUTION LINES TO THE SKY-BRIGHTNESS

Band	Δmag
B	0.09
V	0.16
R	0.10
3970/331	0.08
4280/331	0.16
5510/331	0.10
5820/331	0.33

TABLE 4
SUMMARY OF THE NIGHT-SKY SURFACE BRIGHTNESS

Site & Date	U	B	V	R	I	Reference
02/06/2005*	—-	22.42±0.04	21.66±0.15	21.04±0.13	——	
28/08/2005	21.81±0.10	22.22±0.06	21.27±0.18	20.46±0.07	18.27±0.06	
28/03/2006	—-	22.59±0.17	21.67±0.13	21.04±0.14	19.12±0.08	
mean	21.81±0.10	22.41±0.15	21.53±0.18	20.84±0.27	18.70±0.85	
air-mass corrected	22.39±0.10	22.86±0.03	22.01±0.07	21.36±0.11	19.25±0.14	
La Silla 1978		22.8	21.7	20.8	19.5	Mattila et al. (1996)
Kitt Peak 1987		22.9	21.9			Pilachowski et al. (1989)
Cerro Tololo 1987	22.0	22.7	21.8	20.9	19.9	Walker (1987a,88a)
Calar Alto 1990	22.2	22.6	21.5	20.6	18.7	Leinert et al. (1995)
La Palma 1990-92		22.5	21.5			Benn & Ellison (1998a,b)
La Palma 1994-96	22.0	22.7	21.9	21.0	20.0	Benn & Ellison (1998a,b)
Mauna Kea 1995-06		22.8	21.9			Krisciunas (1997)
Paranal 2000-01	22.3	22.6	21.6	20.9	19.7	Patat et al. (2003)
MtGraham 2000-01	22.38	22.86	21.72	21.19		Taylor et al. (2004)
Cerro Pachon 2005	22.1	22.43	21.63		20.3	Walker & Schwarz (2007)

∗ Based on spectrophotometric data obtained with PPAK.

TABLE 5
EXTINCTION COEFFICIENTS AT CALAR ALTO

Wavelength (nm)	κ_λ Summer	κ_λ Winter
380	0.505±0.126	0.375±0.034
436	0.324±0.057	0.223±0.022
500	0.216±0.049	0.144±0.010
671	0.109±0.034	0.055±0.005
880	0.065±0.017	0.024±0.001
1020	0.049±0.019	0.014±0.002

TABLE 6
CONTRIBUTION OF THE RAYLEIGH SCATTERING (f_1), AEROSOL EXTINCTION (f_2) AND OZONE ABSORPTION (f_2) TO THE
TOTAL EXTINCTION.

Site	height[m]	f_1	f_2	f_3	reference
Calar Alto (Winter)	2168	1.02	0.94	0.29	this work
Calar Alto (Summer)	2168	1.18	4.52	0.19	" "
Calar Alto (Winter)	2168	1.25	1.00	0.00	Hopp & Fernandez (2002)
Lick	1290	1.25	0.80	0.00	" " ∗
Palomar	1706	1.65	0.35	0.03	" " ∗
KPNO	2120	1.40	0.75	0.00	" " ∗
CTIO	2215	1.50	1.10	0.00	" " ∗

(*) Data collected by Hopp & Fernandez (2002) from different studies.

TABLE 7
MEDIAN SEEING COMPARED WITH OTHER ASTRONOMICAL SITES

Site	Median seeing	Reference
Calar Alto (all)	0.90″	this work
Calar Alto (Winter)	0.96″	" "
Calar Alto (Summer)	0.87″	" "
Mauna Kea (1987)	0.50″	Racine (1989)
La Palma (1997)	0.76″	Muñoz-Tuñon et al. (1997)
La Silla (1999)	0.79″	ESO webpage*
Paranal (2005)	0.80″	ESO webpage**
MtGraham (1999-2002)	∼0.97″	Taylor et al. (2004)
Paranal (2006)	∼1.00″	ESO webpage***
KPNO (1999)	∼1.00″	Massey et al. (2000)
Lick (1990-1998)	∼1.90″	MtHamilton webpage****

(*) http://www.ls.eso.org/lasilla/seeing/
(**) http://www.eso.org/gen-fac/pubs/astclim/paranal/seeing/adaptive-optics/statfwhm.html
(***) http://www.eso.org/gen-fac/pubs/astclim/paranal/seeing/singstory.html
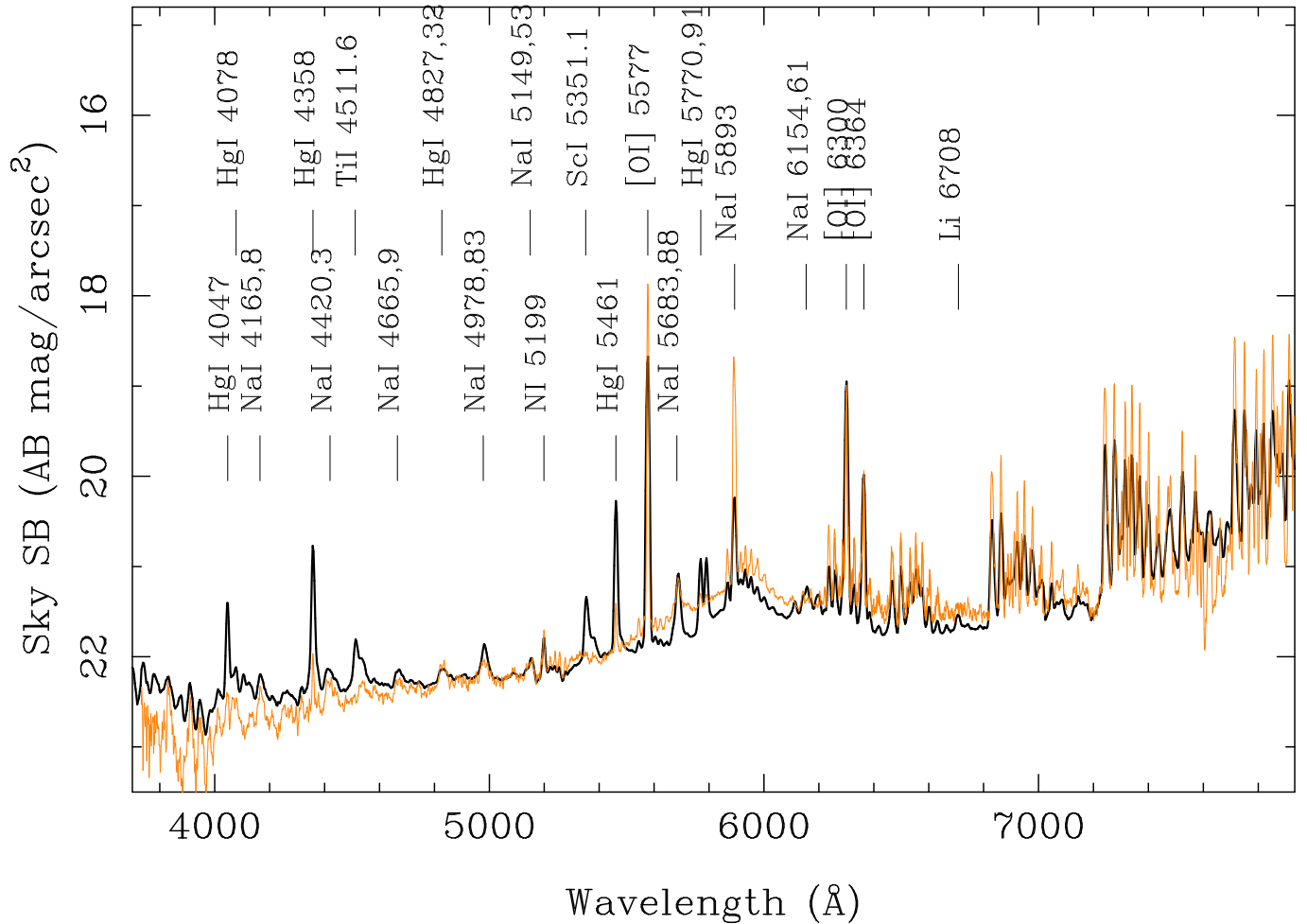(****) https://mthamilton.ucolick.org/techdocs/MH_weather/obstats/seeing.html

FIG. 1.— Night-sky spectrum at the Calar Alto Observatory in the optical wavelength range (3700-7950Å), obtained after averaging 10 spectra of 6 moonless nights pointing near the zenit (Black solid-line). The intensity has been scaled to that of the darkest moonless night in the *V*-band. Several emission lines are indentified in the spectrum. The most relevant ones have been labeled with its corresponding name and wavelength. In addition, the broad-emission band of NaI centred at ∼5900Å, and the water vapor Meinel bands are clearly identified in the spectrum. For comparison purposes we included the night sky spectrum at the Kitt Peak observatory derived by Massey & Foltz (2000), obtained from their webpage: *http://www.lowell.edu/users/massey/nightsky.html* (Orange dotted-line). It is appreciated how strong are the pollution lines at Calar Alto, in comparison with that observatory.
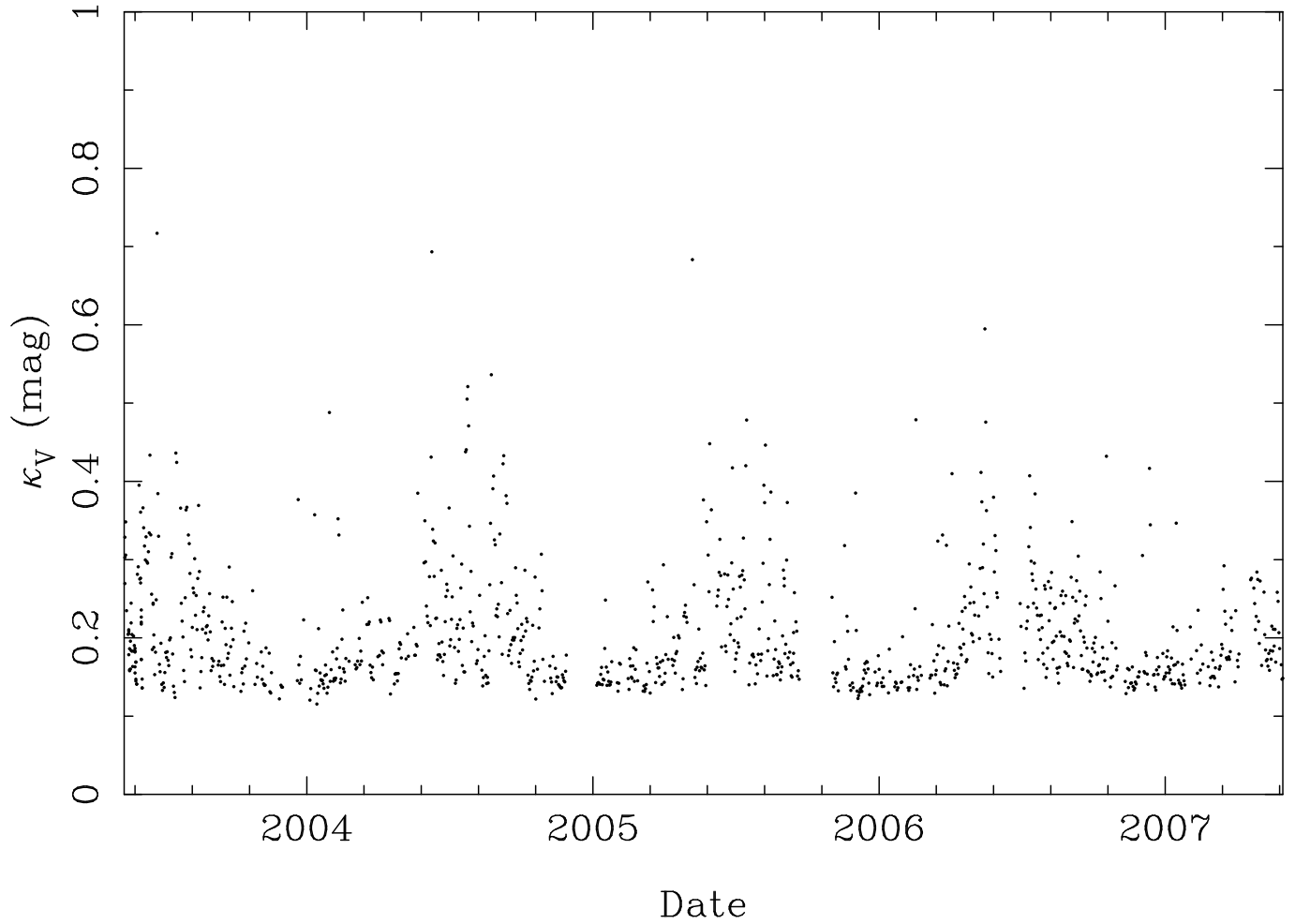
Fig. 2.— Distribution of the V-band extinction along 1044 astronomical useful nights in the period between march 2003 and may 2007 (∼70% of the total nights). The extinction shows a clear seasonal pattern, with a maximum in Summer and a minimun in Winter. The median value of the extinction is κ_V=0.18 mags, with a typical value of ∼0.15 mags in Winter. The fraction of nights with κ_V >0.25 mags, ∼20%, is similar to other observatories (e.g., La Palma), although the peaks of extinction are much lower.
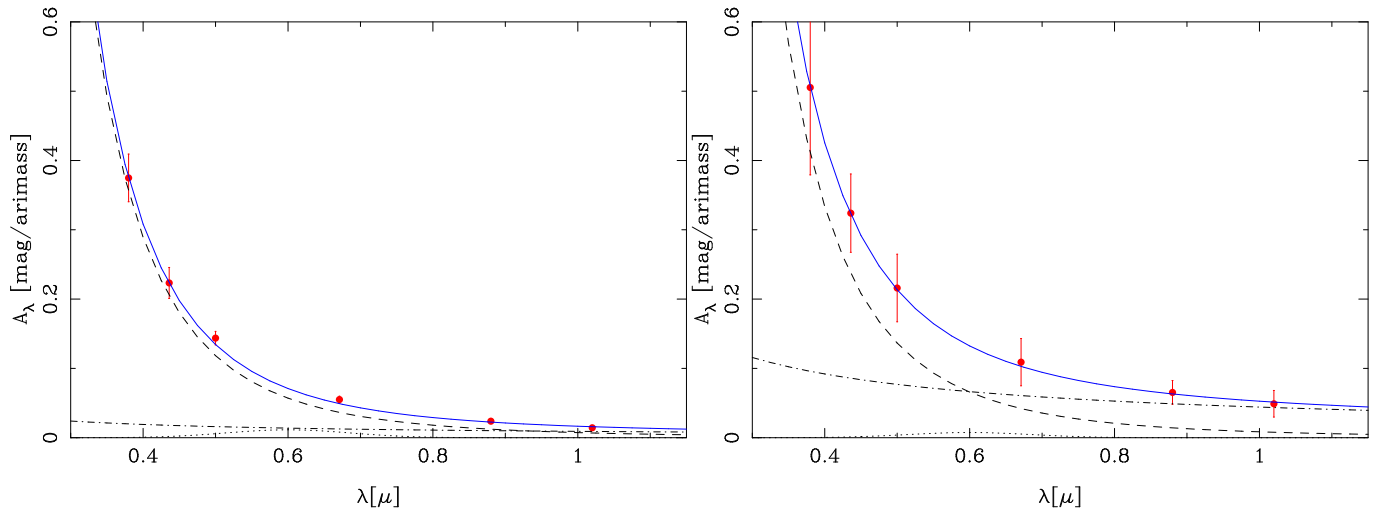
Fig. 3.— Extinction curves derived for a set of Winter (left panel) and summer nights (right panel), using the EXCALIBUR extintion curve monitor (red solid circles). The error bars indicate the standard deviation over the mean values. The data were fitted to a linear combination of the three different contributions to the extinction described in Walker (1987): the Rayleigh scattering (dashed line), the Aerosol or dust extinction (dotted-dashed line), and the Ozone extinction (dotted line), each one scaled to their relative contribution to the extinction. The blue solid line shows the best fit to the data.
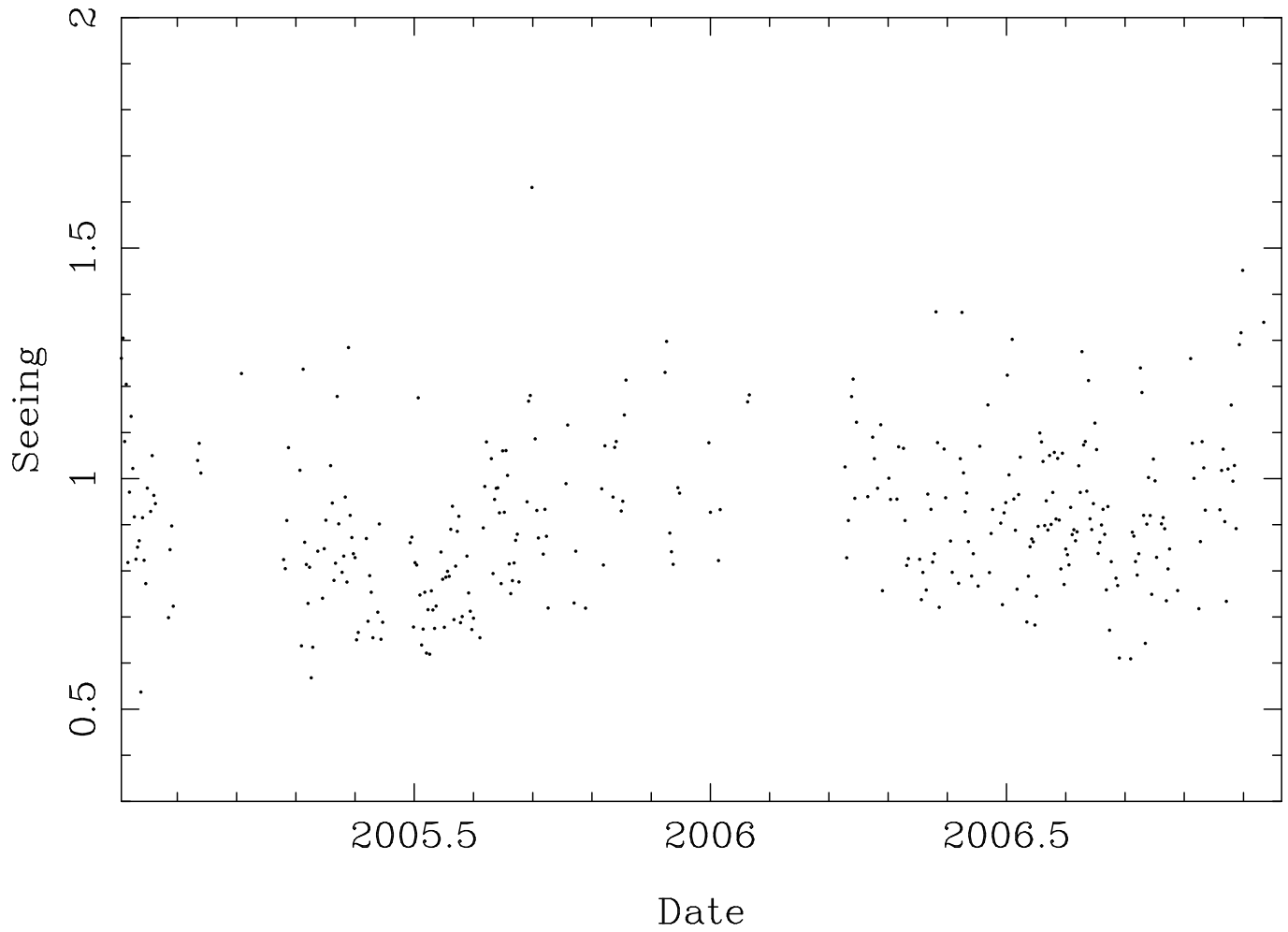
FIG. 4.— Distribution of the seeing along the time for the 335 nights with measurements from the DIMM monitor in the period between January 2005 and December 2006. There is a suggestion for a seasonal pattern, with a minimun during Summer and a maximum during Winter.
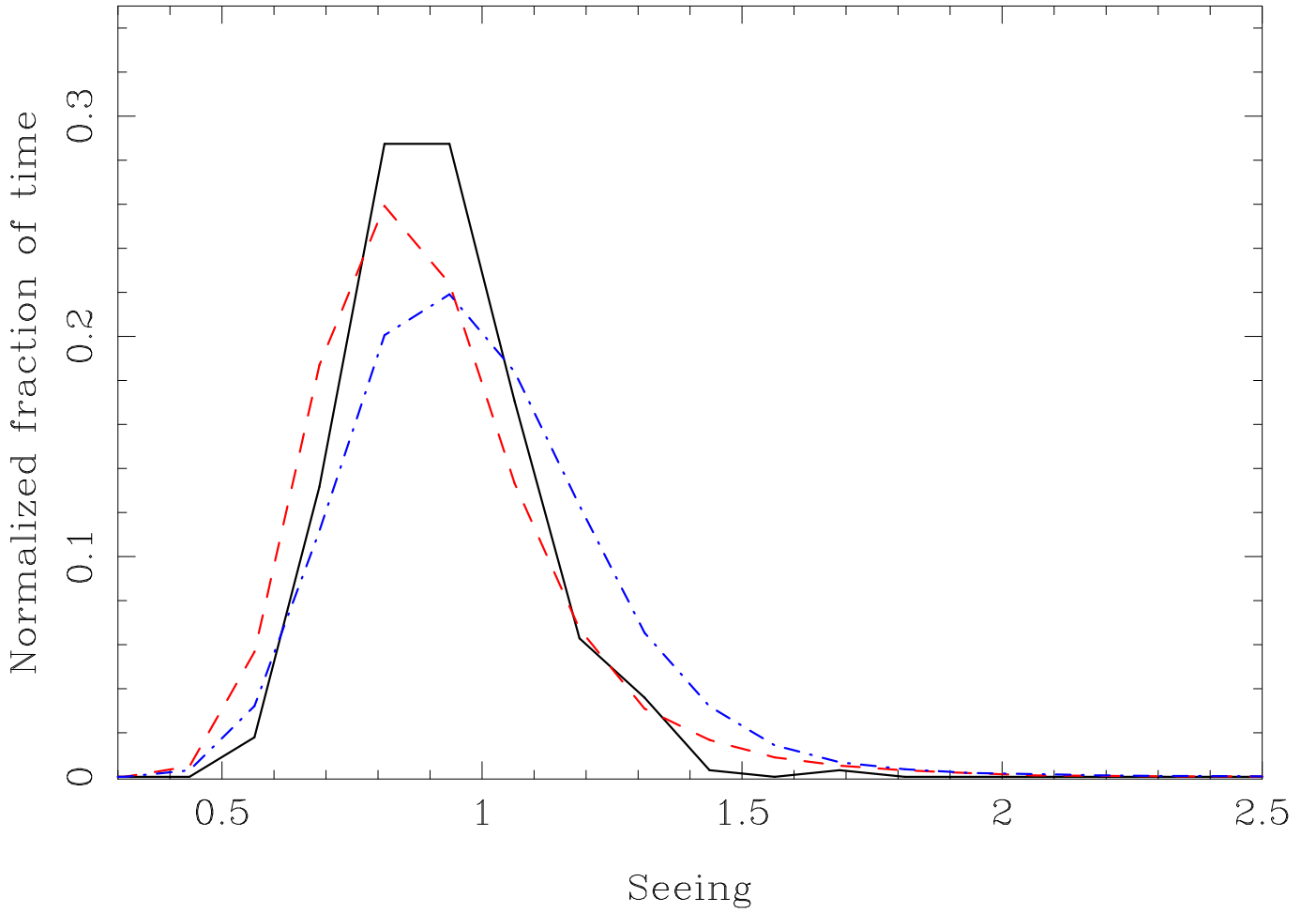
Fig. 5.— Normalized histogram of the seeing distribution shown in Fig.4 (solid line). The median value of the seeing is ∼0.90″, with a ∼46% of the nights with a seeing better than this value. The red dashed line shows a similar histogram for the summer values (May to September), when the median seeing drops to ∼0.87″. The blue dashed-dot line shows a similar histogram for the Winter values, comprising the remaining data, when the median seeing rise to ∼0.96″. The seeing distribution is clearly different in both seasons.